Research Article | Vol. 30, No. 22 / 24 Oct 2022 / Optics Express 40968
Optics EXPRESS

Photon path distributions in optically thin slabs

QUENTIN LIBOIS[1,*] AND ANTHONY B. DAVIS[2]

[1] CNRM, Université de Toulouse, Météo-France, CNRS, Toulouse, France
[2] NASA Jet Propulsion Laboratory, California Institute of Technology, Pasadena, CA, USA
[*] quentin.libois@meteo.fr

Abstract: The probability distribution function of photon path length in a scattering medium contains valuable information on that medium. While strongly scattering optically thick media have been extensively studied, in particular, with resort to the diffusion approximation, optically thin media have received much less attention. Here, we derive the probability distribution functions for the lengths of singly- and twice-scattered photon paths in an isotropically scattering slab of optical thickness τ, for both reflected and transmitted photons. We show that, in the case of an optically thin slab, these photons dominate the overall response of the medium. We confirm that the second moment of the distribution deviates from the ballistic limit in the case of collimated illumination. Interestingly, we show that under diffuse illumination, the second moment of the distribution is dominated by unscattered transmitted photons, hence is proportional to $\ln\tau$, and independent of the phase function. Higher moments of order n ($\geq$3) scale as $H^n\tau^{n-2}$. When only reflected or transmitted photons are considered, the second moment scales as $H^2\tau^{-1}$, whatever the illumination and viewing conditions. This provides direct access to τ. These theoretical results are extensively supported by Monte Carlo ray-tracing simulations. Extension to anisotropic scattering using these same simulations shows that the results hold, given a scaling factor for collimated illumination, and without any dependence on the phase function for diffuse illumination. These results overall demonstrate that the optical thickness of an optically thin slab can be estimated from the second moment of the distribution. Along with the fact that under diffuse illumination the geometrical thickness can be derived from the first moment of the distribution, this proves that the extinction coefficient of the medium can be estimated from the combination of both moments. This study thus opens new perspectives for non-invasive characterization of optically thin media either in the laboratory or by remote sensing.

© 2022 Optica Publishing Group under the terms of the Optica Open Access Publishing Agreement

1. Introduction

Detailed analysis of light scattered by a medium is at the core of several measurement techniques in a variety of areas ranging from atmospheric remote sensing to medical imaging. In many practical situations, the probed medium can be represented as a homogeneous horizontally infinite slab. In this case the main properties that describe the medium are its geometrical thickness H, its extinction and absorption coefficients σ_e (corresponding to a mean free path l_e) and σ_a, and its scattering phase function P (often reduced to the asymmetry parameter g). Generally, reflectance or transmittance is measured, under various illumination and viewing conditions, at a variety of wavelengths and spectral resolutions. In scattering media, photons follow tortuous paths before being eventually absorbed, transmitted or reflected. The diversity of possible paths can be represented by the probability distribution (hereafter called "pdf") of total path length l. Investigation of the path length distribution has been a critical issue for decades [1].

The pdf of photon path length for reflected and transmitted light can be directly measured using photon time-of-flight spectroscopy [2,3] but this requires knowledge of the effective refractive index of the medium [4] and a sophisticated experimental setup that can hardly be deployed. The pdf can also be determined theoretically for certain geometries, considering successive orders of scattering [5], or by using the fact that spectral reflectance and transmittance can be

#464033 https://doi.org/10.1364/OE.464033
Journal © 2022 Received 17 May 2022; revised 1 Jul 2022; accepted 2 Jul 2022; published 21 Oct 2022

Optics EXPRESS

written as the Laplace transform of the path length distribution [6,7], a relationship known as equivalence theorem [8]. The latter method can be applied to analytically derived expressions of reflectance and transmittance [9], or, at least in theory, to observations. However the spectral resolution and noise level required to obtain a satisfactory inversion remain very demanding for real measurements [10]. Although the full pdf contains a wealth of information on the medium [11], in most cases only some moments are accessible, for instance exploiting the Laplace transform results in the moments being related to the derivatives of the measured quantities with respect to σ_a [12]. Hence it is worth investigating how the moments of the pdf are related to the medium characteristics. To do so, one can either assume a particular pdf and fit free parameters in order to match observations [13], or use measurements that are directly related to these moments. For instance, the first moment, namely the mean path length, is what determines overall absorption in the case of weak absorption [14].

Theoretical work has demonstrated that the mean path length of photons escaping from a non-absorbing slab illuminated by a diffuse source equals $2H$, independently of the scattering properties of the medium [15], a property that has been later on verified experimentally [16]. Similar invariance properties have been obtained for higher moments [17], but only in the case of optically thick media. More generally, the diffusion approximation has been widely used to investigate the pdf and its moments [18,19]. This approximation has proven very efficient for optically thick media but is inappropriate for optically thin media, that is, in the ballistic limit. Optically thin media are found everywhere, though, from thin cirrus clouds to human tissues, and deserve more attention.

To model the response of optically thin media to a light beam, various strategies have been explored [20]. Simple models where light can only be scattered perpendicular or parallel to the slab have been used [21,22]. It was shown that the mean path length tends towards $3H$ for normal illumination and low optical thickness, while the ballistic limit would suggest it equals H. This deviation was attributed to the very few photons scattered parallel to the slab, which experience such long paths that this overcompensates their scarceness. In such configuration, it was also found that directly transmitted, reflected and transmitted photons equally contribute to the mean path length. Normal illumination was also considered in [21], but with isotropic scattering in the medium. The pdf of the directly transmitted and singly-scattered (reflected or transmitted) photons was derived, to obtain a lower bound of the successive moments. It was shown that the first moment converges to the ballistic limit H, but that the second moment converges to something larger than H^2, and that the n^{th} moments (n>2) divided by H^n even diverge with decreasing optical thickness τ. In a complementary study [23], this divergence was further explored and it was fully explained by the long tail of the pdf for photons experiencing one or two scattering events. The latter study provides an insightful discussion on the reasons why photons scattered once and twice should equally contribute to the moments divergence.

In the present study, we extend the work of [23] to the general cases of collimated (from any direction) and diffuse illumination. The case of diffuse illumination is of particular interest because of the invariance properties that arise in such conditions. The invariance property for the mean path length has been proven for any optical thickness. In contrast, the dependence of the second moment (the variance) on optical thickness has only been studied in the case of optically thick media. For instance, its quadratic dependence has been derived theoretically in the diffusion limit [19] and observed for transmitted sunlight through opaque stratus clouds [24]. The question naturally arises how the variance behaves in the case of optically thin media. That is a central motivation for the present study, which also advances our understanding of light scattering in optically thin media.

In Section 2, the pdf for singly- and twice-scattered photons are obtained for collimated and diffuse illumination, and for directional and angularly integrated viewing configurations. Focusing on the long tails of these pdf the asymptotic behavior of the moments at low optical

Optics EXPRESS

thickness are investigated. In Section 3, Monte Carlo ray-tracing simulations are performed to validate the analytical results, and to extend the conclusions drawn from the calculations to higher orders of scattering and anisotropic scattering (addressed theoretically in Appendix B). Some practical implications of the present study are discussed in Section 4, and we draw our conclusions in Section 5.

2. Analytical computations

Let us consider a horizontally infinite, homogeneous, purely scattering (i.e., non-absorbing) slab of thickness H illuminated by a beam of photons incident at a zenith angle θ_0 such that $\cos\theta_0 = \mu_0$ ($s_0 = \mu_0^{-1}$). The medium is characterized by its extinction coefficient σ_e, the corresponding extinction length being denoted l_e. The optical thickness of the slab is defined as $\tau = H/l_e$. Let us further assume that the distribution of the photon free path L between two scattering events follows a simple exponential law such that:

$$p(L) = \frac{1}{l_e} e^{-\frac{L}{l_e}}. \tag{1}$$

Let l be the total path length of a photon in the slab between its entrance and escape points (corresponding either to transmitted or reflected paths), and $p(l)$ the corresponding pdf. $p(l)$ can be written as a sum on the number of scattering events experienced by the photons, so that:

$$p(l) = \sum_0^\infty p_k(l), \tag{2}$$

where $p_k(l)$ is the joint probability that a photon has traveled a total length l in the slab and experienced k scattering events. We note $l_0, l_1, \ldots, l_k$ the successive individual contributions to l for a photon that is scattered k times, and θ_k the zenith angle corresponding to l_k. We also note $z_0, \ldots, z_k$ the depth of the $(k+1)^{\text{th}}$ scattering event. Scattering is assumed isotropic within the medium, such that the scattering phase function in terms of the zenith and azimuth angles θ and ϕ is given by $P(\theta, \phi) = \frac{1}{4\pi}$. Because the total distance traveled does not depend on the successive ϕ directions, the probability to be scattered with a zenith angle θ is defined as:

$$P(\theta) = \int_0^{2\pi} P(\theta, \phi) \sin\theta \mathrm{d}\phi = \frac{1}{2} \sin\theta, \tag{3}$$

and is normalized such that $\int_0^\pi P(\theta)\mathrm{d}\theta = 1$. In the following we only focus on $p_0(l)$, $p_1(l)$ and $p_2(l)$. These pdfs are derived for collimated (i.e., when photons come from a single direction) and diffuse (i.e., isotropic) illumination. The focus is first on all escaping photons, whatever their escape direction. Then directional viewing configurations are considered. Figure 1 summarizes the geometry of the problem for single and double scattering.

2.1. Collimated illumination

The case of normal illumination ($\theta_0 = 0$) has already been treated [21,23]. Here we extend the computation to any incident angle θ_0. In this case $p_0(l)$, which corresponds to directly transmitted photons, simply reads:

$$p_0(l) = e^{-\tau s_0} \delta\left(l - H s_0\right), \tag{4}$$

where δ is the Dirac function. To compute $p_1(l)$, the contributions of transmitted and reflected photons are treated separately, and denoted $p_{1,t}(l)$ and $p_{1,r}(l)$.

Optics EXPRESS

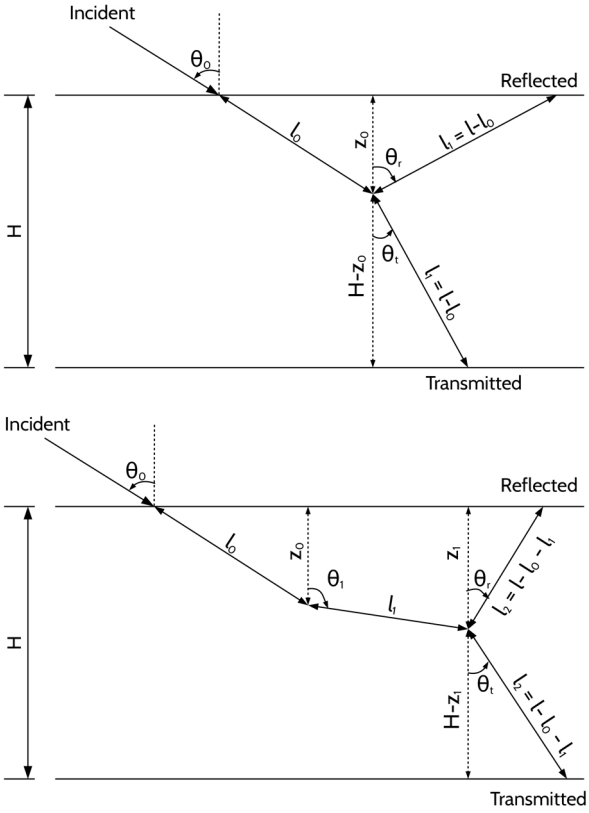

Fig. 1. Geometry of the slab, with the main quantities used in the calculations, for single (top) and double (bottom) scattering.

2.1.1. Singly scattered transmitted photons

The distribution $p_{1,t}(l)$ (equal to 0 for $l \leq H$) can be written as:

$$p_{1,t}(l) = \int_0^H p(z_0)p(l|z_0)\mathrm{d}z_0. \tag{5}$$

Note however that this expression is only valid for $l \geq Hs_0$. In the case $H \leq l \leq Hs_0$ the integral does not extend up to H, it is limited to $z_{\max}$ such that $z_{\max}s_0 + (H - z_{\max}) = l$ (which ensures that $p(l|z_0) \neq 0$), i.e., $z_{\max} = \frac{l-H}{s_0-1}$. As $l_0 = z_0 s_0$, $p(z_0) = p(l_0)s_0 = \frac{s_0}{l_e}e^{-\frac{l_0}{l_e}}$. It's also worth noting that the probability $p(l|z_0)\mathrm{d}l$ equals the probability to be scattered in the direction θ_t, namely $P(\theta_t)\mathrm{d}\theta_t$, times the probability to reach the lower boundary without being scattered again, $e^{-\frac{l-l_0}{l_e}}$. θ_t is the angle ensuring that $l_0 + l_1 = l$, so that $\cos\theta_t = \frac{H-z_0}{l-l_0}$. Differentiating the latter expression gives $\sin\theta_t\mathrm{d}\theta_t = \frac{H-z_0}{(l-z_0s_0)^2}\mathrm{d}l$. Recalling that $P(\theta_t) = \frac{1}{2}\sin\theta_t$, this overall gives:

$$p(l|z_0) = \frac{1}{2}\frac{H - z_0}{(l - z_0 s_0)^2}e^{-\frac{l-l_0}{l_e}}. \tag{6}$$

Finally, for $l \geq Hs_0$:

$$p_{1,t}(l) = \frac{s_0}{2l_e}e^{-\frac{l}{l_e}}\int_0^H \frac{H - z_0}{(l - z_0 s_0)^2}\mathrm{d}z_0 \tag{7}$$

Optics EXPRESS

$$= \frac{\mu_0}{2l_e} e^{-\frac{l}{l_e}} \left(-\ln\left(1 - \frac{H}{\mu_0 l}\right) - \frac{H}{\mu_0 l} \right). \tag{8}$$

For $H \leq l \leq Hs_0$, integration stops at $z_{\max}$:

$$p_{1,t}(l) = \frac{\mu_0}{2l_e} e^{-\frac{l}{l_e}} \left(-\ln\left(\frac{H - \mu_0 l}{(1-\mu_0)l}\right) + \frac{l - H}{\mu_0 l} \right). \tag{9}$$

2.1.2. Singly scattered reflected photons

The distribution $p_{1,r}(l)$ can be written as $p_{1,t}(l)$ in Eq. (5). Like previously the paths $l \geq H(1+s_0)$ (which can be obtained for any z_0), and those such that $l \leq H(1+s_0)$ (which can be obtained only if $z_0 \leq z_{\max}$) are distinguished. Here $z_{\max}$ is such that $l = z_{\max}(1+s_0)$, i.e., $z_{\max} = \frac{l}{1+s_0}$. Defining the escape angle θ_r, $\cos\theta_r = \frac{z_0}{l-l_0}$, and $\sin\theta_r \mathrm{d}\theta_r = \frac{z_0}{(l-z_0 s_0)^2}\mathrm{d}l$. $p(l|z_0)$ now reads:

$$p(l|z_0) = \frac{1}{2} \frac{z_0}{(l - z_0 s_0)^2} e^{-\frac{l-l_0}{l_e}}. \tag{10}$$

Hence for $l \geq H(1+s_0)$:

$$p_{1,r}(l) = \frac{s_0}{2l_e} e^{-\frac{l}{l_e}} \int_0^H \frac{z_0}{(l - z_0 s_0)^2} \mathrm{d}z_0 \tag{11}$$

$$= \frac{\mu_0}{2l_e} e^{-\frac{l}{l_e}} \left(\frac{H}{\mu_0 l - H} + \ln\left(1 - \frac{H}{\mu_0 l}\right) \right). \tag{12}$$

For $l \leq H(1+s_0)$, integration stops at $z_{\max}$ and:

$$p_{1,r}(l) = \frac{\mu_0}{2l_e} e^{-\frac{l}{l_e}} \left(\frac{1}{\mu_0} + \ln\left(\frac{\mu_0}{1+\mu_0}\right) \right). \tag{13}$$

The distributions $p_{1,t}(l)$ and $p_{1,r}(l)$ are shown in Fig. 2 for $H = 2$ m, $\tau = 2$ and $\mu_0 = 0.5$ (black lines). For $\mu_0 = 1$, it can be verified that these equations correspond to previously derived expressions [21].

2.2. Diffuse illumination

We now consider isotropic illumination, such that the pdf of the incident direction of the photons is given by $P(\theta_0, \phi) = \frac{\cos\theta_0}{\pi}$. As a consequence $P(\theta_0) = 2\cos\theta_0 \sin\theta_0$. In this case the pdf of l for directly transmitted photons (equal to 0 for $l \leq H$) is such that:

$$p_0(l)\mathrm{d}l = e^{-\frac{l}{l_e}} P(\theta_l)\mathrm{d}\theta_l; \tag{14}$$

$$p_0(l) = \frac{2H^2 e^{-\frac{l}{l_e}}}{l^3}, \tag{15}$$

where θ_l is such that $\cos\theta_l = \frac{H}{l}$, and $\sin\theta_l \mathrm{d}\theta_l = \frac{H}{l^2}\mathrm{d}l$. As previously, the contributions of singly-scattered photons are separated into the transmitted and reflected paths.

2.2.1. Singly scattered transmitted photons

Following Eq. (5):

$$p_{1,t}(l) = \int_0^{\pi/2} \int_0^H p(\theta_0) p(z_0|\theta_0) p(l|z_0) \mathrm{d}z_0 \mathrm{d}\theta_0, \tag{16}$$

which again is only valid for $l \geq H$. Using $p(z_0|\theta_0)$ and $p(l|z_0)$ as derived in Section 2.1.1:

$$p_{1,t}(l) = \frac{1}{l_e} e^{-\frac{l}{l_e}} \int_0^1 \int_0^H \frac{H - z_0}{(l - z_0/\mu_0)^2} \mathrm{d}z_0 \mathrm{d}\mu_0. \tag{17}$$

With this definition care should be taken for the ranges of integration because short paths are not possible for all θ_0 and all z_0. More precisely, there will be paths for all z_0 only if $l \geq Hs_0$.

Optics EXPRESS

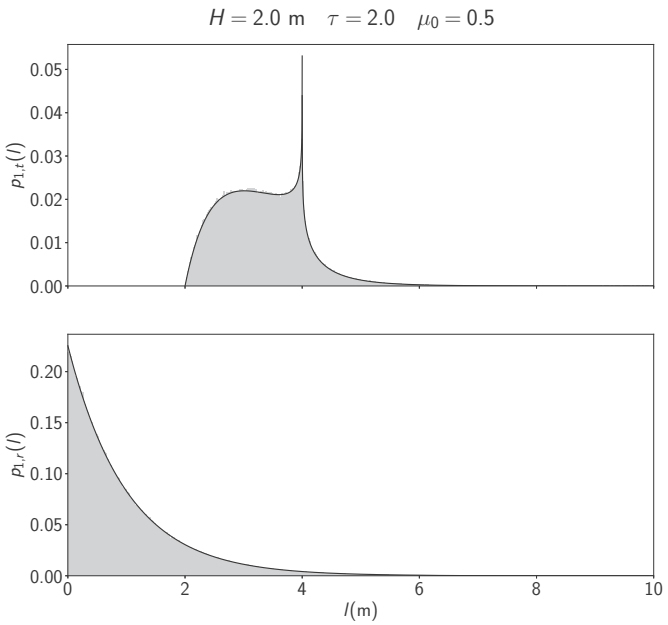

Fig. 2. Probability distributions of total path length for singly scattered transmitted (top) and reflected (bottom) photons under collimated illumination. The black lines correspond to the analytical formulas of Eqs. (8), (9), (12), (13). The gray shades correspond to histograms obtained from Monte Carlo simulations with 10^7 photons launched.

Otherwise, only the z_0 such that $l \geq z_0 s_0 + (H - z_0)$ are possible, i.e., $z_0 \leq \frac{l-H}{s_0-1}$. As a consequence,

$$p_{1,t}(l) = \frac{1}{l_e} e^{-\frac{l}{l_e}} \left[\int_{H/l}^{1} \int_{0}^{H} \frac{H - z_0}{(l - z_0/\mu_0)^2} \mathrm{d}z_0 \mathrm{d}\mu_0 + \int_{0}^{H/l} \int_{0}^{(l-H)/(1/\mu_0 - 1)} \frac{H - z_0}{(l - z_0/\mu_0)^2} \mathrm{d}z_0 \mathrm{d}\mu_0 \right]. \tag{18}$$

These integrals are computed in Appendix A, and the final result is:

$$p_{1,t}(l) = \frac{2}{3l^3 l_e} e^{-l/l_e} \left[H^3 \ln\left(\frac{H}{l} - 1\right) - l^3 \ln\left(1 - \frac{H}{l}\right) + H^2 l - H l^2 \right]. \tag{19}$$

2.2.2. Singly scattered reflected photons

We proceed similarly for the reflected paths to obtain the following expression:

$$p_{1,r}(l) = \frac{1}{l_e} e^{-l/l_e} \int_{0}^{1} \int_{0}^{H} \frac{z_0}{(l - z_0/\mu_0)^2} \mathrm{d}z_0 \mathrm{d}\mu_0. \tag{20}$$

Again care should be taken for the boundaries of integration. Let first consider the paths such that $l \geq 2H$. In this case, all z_0 are possible only if $l \geq H(s_0 + 1)$, that is $\mu_0 \geq \frac{H}{l-H}$. Otherwise, the paths are restricted to those such that $l \geq z_0(s_0 + 1)$, that is $z_0 \leq \dfrac{l}{s_0 + 1}$. For $l \leq 2H$, only the

Optics EXPRESS

second contribution is taken into account. This can be summarized as follows:

$$\underline{\text{if } l \geq 2H:} \qquad p_{1,r}(l) = \frac{1}{l_e} e^{-l/l_e} \left[\int_{H/(l-H)}^{1} \int_0^H \frac{z_0}{(l - z_0/\mu_0)^2} \mathrm{d}z_0 \mathrm{d}\mu_0 + \int_0^{H/(l-H)} \int_0^{l/(1/\mu_0+1)} \frac{z_0}{(l - z_0/\mu_0)^2} \mathrm{d}z_0 \mathrm{d}\mu_0 \right]. \tag{21}$$

$$\underline{\text{if } l \leq 2H:} \qquad p_{1,r}(l) = \frac{1}{l_e} e^{-l/l_e} \int_0^1 \int_0^{l/(1/\mu_0+1)} \frac{z_0}{(l - z_0/\mu_0)^2} \mathrm{d}z_0 \mathrm{d}\mu_0. \tag{22}$$

These integrals are computed in Appendix A, and for $l \geq 2H$ the final result is:

$$\begin{aligned} p_{1,r}(l) = \frac{2}{3l_e} e^{-l/l_e} & \left(\ln\left(1 - \frac{H}{l}\right) + 2\left(\frac{H}{l}\right)^3 \ln\left(\frac{l}{H} - 1\right) \right. \\ & + \frac{H}{l^3} \left[\frac{1}{2} \left((l-H)^2 - \left(\frac{H^2}{l-H}\right)^2 \right) + 2H \left(l - \frac{lH}{l-H} \right) \right] \\ & \left. - \frac{1}{4} \left(\left(\frac{l}{l-H}\right)^2 - 1 \right) + \frac{H}{l-H} + \frac{3}{4} \left(\frac{H}{l-H}\right)^2 \right). \end{aligned} \tag{23}$$

For $l \leq 2H$, the computation simply reads:

$$p_{1,r}(l) = \frac{2}{3l_e} e^{-l/l_e} \left(1 - \ln 2\right). \tag{24}$$

These distributions are shown in Fig. 3 (black lines) for $H = 1$ m and $\tau = 1$.

2.3. *Directional observations with collimated illumination*

The pdfs derived in the previous sections were obtained considering all photons escaping the slab, whatever their escape direction. Although conceptually useful, these pdfs are not applicable to standard satellite or ground observations which generally measure scattered photons at a particular viewing angle, and under collimated illumination (from the Sun or from an active source such as a lidar). Using the same approach as previously the joint probability distribution of l and escape angle (θ_r or θ_t), is derived for both transmitted and reflected photons. As before, this pdf is decomposed in successive orders of scatterings.

2.3.1. Reflected photons

For single scattering, the pdf simply corresponds to the probability to be scattered at the appropriate depth z_0, and then to escape without being scattered again:

$$\begin{aligned} p_{1,r}(l, \theta_r)\mathrm{d}l &= p(z_0)|_{z_0 = \frac{l}{s_0 + s_r}} \mathrm{d}z_0 e^{-\frac{l-l_0}{l_e}} \frac{1}{2} \sin\theta_r; \\ p_{1,r}(l, \theta_r) &= \frac{1}{2l_e} \frac{s_0}{s_0 + s_r} e^{-\frac{l}{l_e}} \sin\theta_r, \end{aligned} \tag{25}$$

where $s_r = \mu_r^{-1}$, and $\mu_r = \cos\theta_r$. Note that the corresponding normalized pdf reads:

$$\overline{p_{1,r}}(l, \theta_r) = \frac{p_{1,r}(l, \theta_r)}{\int_0^{H(s_0+s_r)} p_{1,r}(l, \theta_r)\mathrm{d}l} = \frac{1}{l_e} \frac{e^{-\frac{l}{l_e}}}{1 - e^{-\tau(s_0+s_r)}}, \tag{26}$$

which is consistent with the equation (6.2) of [1].

Optics EXPRESS

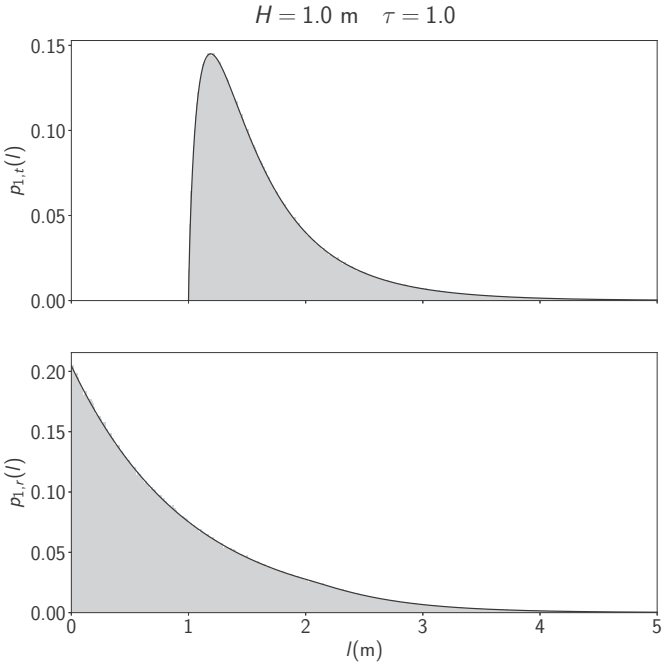

Fig. 3. Same as Fig. 2 but for diffuse illumination. The black lines correspond to the analytical formulas of Eqs. (19), (23), (24).

Singly scattered photons do not correspond to very long trajectories, hence to further investigate long paths it is useful to derive $p_{2,r}(l)$. We first notice that in the case of double-scattering without $l_1 = (z_0 - z_1)s_1$, and $l_2 = z_1 s_r$, where $s_1 = \mu_1^{-1}$, and $\mu_1 = \cos\theta_1$. Also $\mathrm{d}l = \mathrm{d}z_1(s_r - s_1)$.

$$\begin{aligned} p_{2,r}(l,\theta_r) &= \int_0^H p(z_0)\int_0^\pi P(\theta_1)p(l|z_0,\theta_1)\mathrm{d}\theta_1\mathrm{d}z_0, \\ &= \int_0^H p(z_0)\int_0^\pi P(\theta_1)p(z_1)|_{z_1=\frac{l-l_0-z_0s_1}{s_r-s_1}}\frac{1}{|s_r-s_1|}P(\theta_r)e^{-\frac{l-l_0-l_1}{l_e}}\mathrm{d}\theta_1\mathrm{d}z_0, \\ &= \frac{s_0}{4l_e^2}e^{-\frac{l}{l_e}}\sin\theta_r\int_0^H\int_{-1}^1\frac{\mu_r}{|\mu_r-\mu_1|}\mathrm{d}\mu_1\mathrm{d}z_0. \end{aligned} \tag{27}$$

Care should be taken when integrating over μ_1 to ensure that paths exist such that $0 \le z_1 \le H$. We define z_m such that $z_m = \min\left(H, \frac{l}{s_0+s_r}\right)$, the depth (if any) corresponding to single scattering trajectories. If $z_0 \le z_m$ then θ_1 must be larger than θ_r to lengthen the single-scattering path. If $z_0 \ge z_m$ then θ_1 must be smaller than θ_r (i.e., $s_1 \le s_r$). Given that $z_1 = \frac{l-l_0-z_0s_1}{s_r-s_1}$, the above inequalities on z_1 give:

$$\mu_1 \ge \frac{H - z_0}{Hs_r - l + l_0}, \tag{28}$$

$$\text{and} \quad \mu_1 \le \frac{z_0}{l - l_0} \quad \text{for} \quad z_0 \le z_m; \tag{29}$$

$$\mu_1 \ge \frac{z_0}{l - l_0} \quad \text{for} \quad z_0 \ge z_m. \tag{30}$$

Optics EXPRESS

This overall reads:

$$p_{2,r}(l,\theta_r) = \frac{s_0}{4l_e^2} e^{-\frac{l}{l_e}} \sin\theta_r \left[\int_0^{z_m} \int_{\frac{H-z_0}{Hs_r-l+l_0}}^{\frac{z_0}{l-l_0}} \frac{\mu_r}{\mu_r-\mu_1} \mathrm{d}\mu_1 \mathrm{d}z_0 + \int_{z_m}^{H} \int_{\frac{z_0}{l-z_0}}^{1} \frac{\mu_r}{\mu_1-\mu_r} \mathrm{d}\mu_1 \mathrm{d}z_0 \right]. \tag{31}$$

We focus only on long paths such that $z_m = H$ (i.e., $l \geq H(s_0 + s_r)$, meaning that the second scattering without lengthens the single-scattering path ($\mu_1 \geq \mu_r$). The above expression reduces to:

$$\begin{aligned} p_{2,r}(l,\theta_r) &= -\frac{s_0}{4l_e^2} e^{-\frac{l}{l_e}} \sin\theta_r \mu_r \int_0^H \left[\ln\left(\mu_r - \frac{z_0}{l-l_0}\right) - \ln\left(\mu_r - \frac{H-z_0}{Hs_r-l+l_0}\right) \right] \mathrm{d}z_0 \\ &= \frac{s_0}{4l_e^2} e^{-\frac{l}{l_e}} \sin\theta_r \mu_r \int_0^H \ln\left(\frac{l-l_0}{l-l_0-Hs_r}\right) \mathrm{d}z_0 \\ &= \frac{1}{4l_e^2} e^{-\frac{l}{l_e}} \sin\theta_r \mu_r \ln\left((l-Hs_0)^{(Hs_0-l)} (l-Hs_r)^{(Hs_r-l)} (l-H(s_0+s_r))^{(l-H(s_0+s_r))} l^l \right). \end{aligned} \tag{32}$$

For $s_0 = s_r = 1$, this expression is consistent with the equation (6.5) of [1].

2.3.2. Transmitted photons

The same strategy is applied to estimate $p_{1,t}(l,\theta_r)$ and $p_{2,t}(l,\theta_r)$. This reads (for $s_t \neq s_0$):

$$\begin{aligned} p_{1,t}(l,\theta_t) &= p(z_0)|_{z_0=\frac{l-H}{s_0-s_t}} \frac{1}{|s_0-s_t|} e^{-\frac{l_1}{l_e}} \frac{1}{2} \sin\theta_t \\ &= \frac{1}{2l_e} \frac{s_0}{|s_0-s_t|} e^{-\frac{l}{l_e}} \sin\theta_t. \end{aligned} \tag{33}$$

The corresponding normalized pdf reads:

$$\overline{p_{1,t}}(l,\theta_t) = \frac{1}{l_e} \frac{e^{-\frac{l}{l_e}}}{|e^{-\tau s_0} - e^{-\tau s_t}|}, \tag{34}$$

which again agrees with equation (6.3) of [1].

For double scattering the strategy is the same as for reflected photons, except that the integration bounds are different. Noticing that $z_1 = \frac{Hs_t + z_0 s_1 - l + l_0}{s_1 + s_t}$, the conditions $0 \leq z_1 \leq H$ become:

$$\frac{z_0 - H}{l - l_0} \leq \mu_1 \leq \frac{z_0}{l - Hs_t - l_0}. \tag{35}$$

The pdf for sufficiently long paths is given by:

$$\begin{aligned} p_{2,t}(l,\theta_t) &= \frac{s_0}{4l_e^2} e^{-\frac{l}{l_e}} \sin\theta_t \int_0^H \int_{\frac{z_0-H}{l-l_0}}^{\frac{z_0}{l-Hs_t-l_0}} \frac{\mu_t}{\mu_t+\mu_1} \mathrm{d}\mu_1 \mathrm{d}z_0, \\ &= \frac{1}{4l_e^2} e^{-\frac{l}{l_e}} \sin\theta_t \mu_t \ln\left((l-Hs_0)^{(Hs_0-l)} (l-Hs_t)^{(Hs_t-l)} (l-H(s_0+s_t))^{(l-H(s_0+s_r))} l^l \right). \end{aligned} \tag{36}$$

Note that this expression only holds for $l \geq H(1 + s_0 + s_t)$, which ensures that the upper limit of the integral $\frac{z_0}{l-Hs_t-l_0} \leq 1$. Interestingly, it means that for long paths, when two scatterings occur, the probability to be reflected in a direction equals that of being transmitted in the symmetrical direction. This is consistent with Table 1 of [1] which shows that for an optical thickness of 0.1 the contributions of scattered transmitted and reflected photons to the mean path are similar. The black lines in Fig. 4 show the behavior of $p_{2,r}(l,\theta_r)$ and $p_{2,t}(l,\theta_t)$ for large l values.

Optics EXPRESS

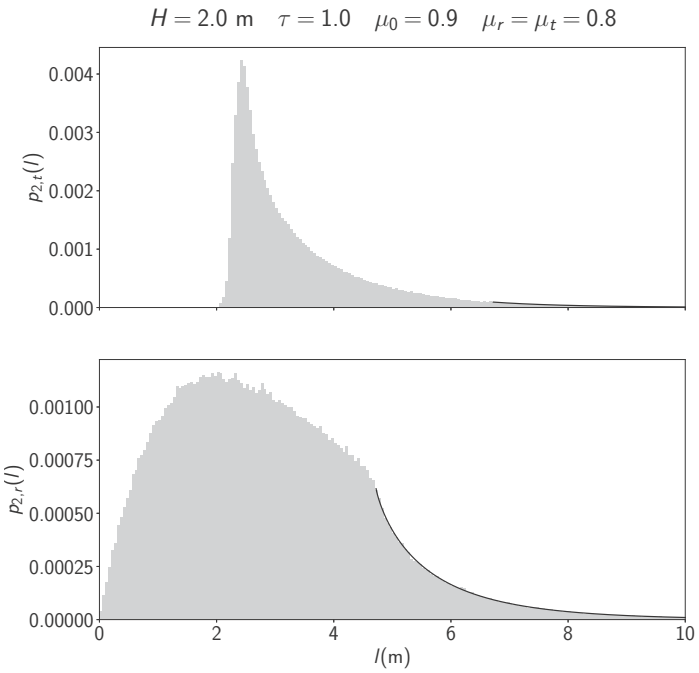

Fig. 4. Same as Fig. 2 but for directional viewing. The black lines correspond to the analytical formulas of Eqs. (32), (36). The histograms are obtained from Monte Carlo simulations with 10^8 photons launched.

2.3.3. Specific case of nadir illumination and viewing

Although we did not derive the general expressions of $p_{2,t}(l, \theta_r)$ and $p_{2,r}(l, \theta_r)$ for low values of l, we provide below the expression for nadir illumination and viewing, which corresponds to backscattering measurements, for instance corresponding to monostatic lidar observations. In this case, for $l \leq 2H$:

$$p_{2,r}(l, \theta_r) = \frac{1}{4l_e^2} e^{-\frac{l}{l_e}} \sin\theta_r l \ln 2, \tag{37}$$

where $\theta_r \ll 1$. This expression is consistent with equation (6.5) of [1].

3. Estimation of the moments

In this section the moments of the previously derived pdfs are estimated. The n^{th} moment is denoted $M_{i,x}^{(n)}$, where the lowerscript refers to the pdf of interest. The moments for collimated normal illumination ($\mu_0 = 1$) have already been investigated in [21,23]. The authors concluded that in the case of an optically thin slab, $M^{(n)}$ differs from the ballistic limit H^n as soon as $n \geq 2$, and the normalized moments $M^{(n)}/H^n$ even diverge as τ^{n-2} for $n \geq 3$. They attributed this to the few photons being scattered nearly parallel to the slab boundaries that would experience very long paths. These photons, making up the long tail of the pdf, would not affect the mean path but would drive the divergence for higher moments. In addition, they provided physical insight to support the fact that the moments of $p(l)$ would be dominated in such conditions by the contributions of $p_0(l)$, $p_1(l)$, and $p_2(l)$, with the contributions of photons scattered once and twice being of the same order of magnitude. Their theoretical results were supported by Monte Carlo ray tracing simulations. Here we investigate the moments of $p_0(l)$ and $p_1(l)$ in the case of collimated illumination for any incident direction, and for diffuse illumination. We

Optics EXPRESS

also investigate the moments of $p_2(l)$ for the case of directional observations. The main focus is on the behavior of the normalized moments at low optical thickness, a normalized moment corresponding to the moment divided by the ballistic moment, i.e., $(H/\mu_0)^n$ for direct illumination and $(2H)^n$ [15] for diffuse illumination.

3.1. Collimated illumination

For low optical thickness the contribution of the unscattered transmitted photons to $M^{(n)}$ simply becomes $(H/\mu_0)^n$. For singly-scattered photons, using only the expressions of Eqs. (8) and (12) valid for $l \geq 2H$, the pdfs reduce to (for $\mu_0 l \gg H$):

$$p_{1,t}(l) \sim p_{1,r}(l) \sim \frac{1}{4\mu_0 l_e} e^{-l/l_e} \left(\frac{H}{l}\right)^2, \tag{38}$$

so that the second normalized moment simply reads:

$$\frac{\mu_0^2 M_{1,t}^{(2)}}{H^2} \sim \frac{\mu_0^2 M_{1,r}^{(2)}}{H^2} \sim \frac{\mu_0}{4}. \tag{39}$$

For $\mu_0 = 1$ this suggests that the second normalized moment for transmitted photons which have encountered one scattering or less is 1.25, which is consistent with the Fig. 3 of [21]. For higher moments:

$$\frac{\mu_0^n M_{1,t}^{(n)}}{H^n} \sim \frac{\mu_0^n M_{1,r}^{n}}{H^n} \sim \frac{\mu_0^{n-1}}{4} \tau^{2-n} \Gamma(n-1), \tag{40}$$

where Γ is the gamma function and $\Gamma(n) = (n-1)!$.

3.2. Diffuse illumination

Starting from Eq. (15), $M_{0,t}^{(0)} = 2\tau^2 \Gamma(-2, \tau)$, where we've used the standard notation for the incomplete Γ function. Likewise,

$$\frac{M_{0,t}^{(1)}}{2H} = \tau \Gamma(-1, \tau), \quad ; \quad \frac{M_{0,t}^{(2)}}{4H^2} = \frac{1}{2}\Gamma(0, \tau). \tag{41}$$

From the asymptotic behavior of the incomplete gamma function when $\tau \to 0$:

$$M_{0,t}^{(0)} \sim 1 \quad ; \quad \frac{M_{0,t}^{(1)}}{2H} \sim 1 \quad ; \quad \frac{M_{0,t}^{(2)}}{4H^2} \sim -\frac{1}{2} \ln \tau. \tag{42}$$

The behavior of $M_{0,t}^{(0)}$ simply means that for a sufficiently optically thin slab, the probability to be transmitted without being scattered approaches 1. The asymptotic behavior of $M_{0,t}^{(1)}$ is consistent with the invariance property of the mean path length for diffuse illumination [15], which applied to a non-scattering slab states that the mean path length equals $2H$. Finally the behavior of $M_{0,t}^{(2)}/4H^2$ shows a divergence as $\ln \tau$. It suggests that the infinitely long trajectories through the slab corresponding to grazing angles dominate the variance of the paths, although they are

Optics EXPRESS

extremely rare. Extension to higher moments reads for $n \geq 3$:

$$\frac{M_{0,t}^{(n)}}{2^n H^n} \sim \frac{1}{2^{n-1}} \tau^{2-n} \Gamma(n-2). \tag{43}$$

We now investigate the contribution of the scattered photons. Like previously, we keep only the dominant term of $p_{1,t}(l)$:

$$p_{1,t}(l) \sim \frac{1}{l_e} e^{-l/l_e} \left(\frac{H}{l}\right)^2, \tag{44}$$

so that as $\tau \to 0$,

$$\frac{M_{1,t}^{(2)}}{4H^2} \sim \frac{1}{4}. \tag{45}$$

Interestingly the contributions of I_1 and I_2 in Eqs. (67) and (68) are equal, meaning that grazing angles contribute as much as non-grazing angles. Similarly it can be shown that $M_{1,r}^{(2)}/4H^2 \sim 1/4$, and that again the contributions are equally split between grazing and non-grazing incident angles. These results demonstrate that the singly-scattered photons do not contribute to the divergence of $M^{(2)}/4H^2$, which is only due to the unscattered photons. Assuming that twice-scattered photons and higher orders do not contribute to the divergence either, it suggests that the asymptotic behavior of $M^{(2)}/4H^2$ is dominated by unscattered photons, hence is independent of the scattering phase function, which provides a direct way of estimating τ without any information on the phase function. Like previously, extension to higher moments directly reads:

$$\frac{M_{1,t}^{(n)}}{2^n H^n} \sim \frac{M_{1,r}^{(n)}}{2^n H^n} \sim \frac{1}{2^n} \tau^{2-n} \Gamma(n-1). \tag{46}$$

3.2.1. Realistic configurations

Measuring all photons escaping from a scattering slab under collimated or diffuse illumination is not a common measurement configuration. More often, the illumination is direct, and only reflected or transmitted radiation is measured (with full angular integration or at a specific viewing angle). In such case, the relevant pdfs are those corresponding to the actually measured photons. It means that the pdfs presented in Sections 2.1, 2.2, 2.3 should be normalized by the probability of actually being reflected (respectively transmitted), in all directions or in the direction θ_r (respectively θ_t). We do not derive these latter probabilities that aggregate all orders of scattering, but hypothesize that at low optical thickness, they are dominated by single scattering (excluding direct transmission measurements). As previously, the subsequent derivations are obtained in the limit $\tau \to 0$.

Directional reflection. We define the photon path pdf for reflected photons only:

$$\overline{p_{i,r}}(l, \theta_r) = \frac{p_{i,r}(l, \theta_r)}{\int_0^\infty \sum_1^\infty p_{i,r}(l, \theta_r) \mathrm{d}l}. \tag{47}$$

We assume that at low optical thickness the probability of being reflected in direction θ_r equals the probability of single-scattering without:

$$\int_0^\infty \sum_1^\infty p_{i,r}(l, \theta_r) \mathrm{d}l \sim \int_0^{H(s_0+s_r)} p_{1,r}(l, \theta_r) \mathrm{d}l \sim \frac{1}{2\mu_0} \tau \sin\theta_r. \tag{48}$$

As a consequence:

$$\overline{p_{1,r}}(l, \theta_r) \sim \frac{e^{-\frac{l}{l_e}}}{H(s_0 + s_r)}. \tag{49}$$

Optics EXPRESS

From this pdf, the normalized moments for singly-scattered photons can be computed:

$$\frac{M_{1,r}^{(1)}}{H} \sim \frac{1}{2}(s_0 + s_r) \quad ; \quad \frac{M_{1,r}^{(2)}}{H^2} \sim \frac{1}{3}(s_0 + s_r)^2. \tag{50}$$

The expression of $M_{1,r}^{(1)}$ is consistent with the Figs. 5 and 6 of [1]. This suggests that in the case of an optically thin medium, the average photon path length of singly-scattered reflected photons provides an estimate of the slab geometrical thickness. Interestingly, in the case of an optically thick medium, the mean photon path length for all reflected photons under the assumption of isotropic scattering reads [8]:

$$\frac{M^{(1)}}{H} = (\mu_0 + \mu_r), \tag{51}$$

which also highlights a scaling with H.

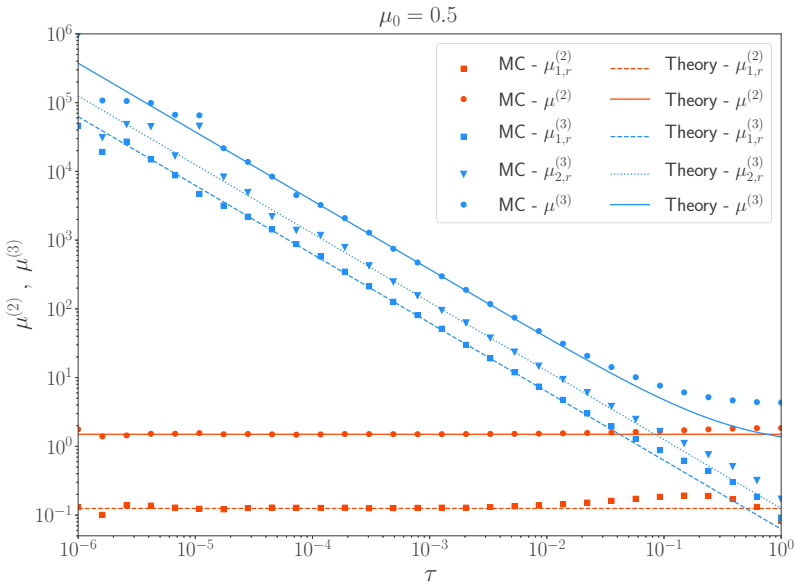

Fig. 5. Second and third normalized moments ($\mu^{(2)} = \mu_0^2 M^{(2)}/H^2$ and $\mu^{(3)} = \mu_0^3 M^{(3)}/H^3$) of $p(l)$ for collimated illumination ($\mu_0 = 0.5$) and istropic scattering, as derived analytically (lines) and obtained with ray tracing simulations (symbols). Note that the moments for transmitted photons are not shown, since they would superimpose with those of reflected photons. Likewise, the second moments for twice-scattered photons are not shown because they would superimpose with those of singly-scattered photons. MC stands for Monte Carlo simulations.

We now focus on $p_{2,r}(l)$. It can be shown that for $l \gg H(s_0 + s_r)$,

$$p_{2,r}(l) \sim \frac{s_0}{4} e^{-\frac{l}{l_e}} \sin\theta_r \frac{\tau^2}{l}, \tag{52}$$

so that,

$$\overline{p_{2,r}}(l, \theta_r) \sim \frac{\tau}{2} \frac{e^{-\frac{l}{l_e}}}{l}. \tag{53}$$

It follows that:

$$\frac{M_{2,r}^{(1)}}{H} \sim \frac{1}{2} \quad ; \quad \frac{M_{2,r}^{(2)}}{H^2} \sim \frac{1}{2\tau}. \tag{54}$$

Optics EXPRESS

It shows that the second normalized moment diverges as τ^{-1} in the limit $\tau \to 0$, implying that the divergence is driven by photons scattered nearly parallel to the slab. Interestingly there is no dependence on the angles of incidence and escape. For higher moments the contribution of twice-scattered photons becomes:

$$\frac{M_{2,r}^{(n)}}{H^n} \sim \frac{1}{2}\tau^{1-n}\Gamma(n). \tag{55}$$

Directional transmission. Proceeding similarly for photons transmitted in direction θ_t:

$$\overline{p_{1,t}}(l, \theta_r) \sim \frac{e^{-\frac{l}{l_e}}}{H|s_0 - s_t|}. \tag{56}$$

From this expression the normalized moments can be computed:

$$\frac{M_{1,t}^{(1)}}{H} \sim \frac{1}{2}(s_0 + s_t) \quad ; \quad \frac{M_{1,t}^{(2)}}{H^2} \sim \frac{1}{3}(s_0^2 + s_0 s_t + s_t^2). \tag{57}$$

Again, the expression for $M^{(1)}$ is consistent with the asymptotic behavior seen in Fig. 7 of [1]. As the asymptotic behavior of $p_{2,t}(l)$ is similar to that of $p_{2,r}(l)$, the corresponding moments also behave similarly:

$$\frac{M_{2,t}^{(1)}}{H} \sim \frac{1}{2} \quad ; \quad \frac{M_{2,t}^{(2)}}{H^2} \sim \frac{1}{2\tau} \quad ; \quad \frac{M_{2,t}^{(n)}}{H^n} \sim \frac{1}{2}\tau^{1-n}\Gamma(n). \tag{58}$$

Note that the independence of $M_{2,t}^{(1)}$ to μ_0 and μ_t appears in the Fig. 7 of [1].

Reflection and transmission in all directions. Building on the previous derivations it is worth considering reflectance and transmittance measurements that account for photons reflected in all directions, under collimated or diffuse illumination. It implies a scaling of the pdfs derived in Sections 2.4.1 and 2.4.2 by the probability to actually be reflected or transmitted, again assumed to be dominated by single-scattering without. In this case, the scaling of $M^{(2)}$ changes. Bearing in mind that the asymptotic expressions are similar for reflected and transmitted photons it reads for collimated illumination:

$$\int_0^\infty p_{1,r}(l)\mathrm{d}l \sim \int_0^\infty p_{1,t}(l)\mathrm{d}l \sim \frac{\tau s_0}{2}, \tag{59}$$

so that:

$$\frac{M_{1,r}^{(2)}}{H^2} \sim \frac{M_{1,r}^{(2)}}{H^2} \sim \frac{1}{2\tau}. \tag{60}$$

Note that there is no dependence on μ_0.

For diffuse illumination:

$$\int_0^\infty p_{1,r}(l)\mathrm{d}l \sim \int_0^\infty p_{1,t}(l)\mathrm{d}l \sim \tau, \tag{61}$$

so that:

$$\frac{M_{1,r}^{(2)}}{4H^2} \sim \frac{M_{1,t}^{(2)}}{4H^2} \sim \frac{1}{4\tau}. \tag{62}$$

These findings suggest that when only reflected or transmitted photons are considered, for directional (respectively angularly integrated) viewing configurations, twice-scattered (respectively singly-scattered) photons contribute to the divergence of the second normalized moment as τ^{-1}.

Optics EXPRESS

4. Monte-Carlo ray-tracing simulations

Now that we have derived analytical expressions for the photons scattered once and twice, we compare these expressions to the results obtained with a Monte Carlo ray tracing code. This code, which is similar in essence to [25], consists in launching a number of photons at the surface of a numerical slab, and following them until they escape the slab via transmission or reflection. The distance between successive scattering events is drawn from the pdf given by Eq. (1) and the scattering angle is drawn from a Henyey–Greenstein phase function [26] described by the asymmetry parameter g. For diffuse illumination the incident angle is drawn from the angular distribution $2\cos\theta\sin\theta$. The code was optimized to work at low optical thickness. To this end, each photon contributes to scattering (the probability to be unscattered is taken into account for each photon), following the strategy of [21]. In addition, for diffuse illumination, more photons are sent with grazing angles to better explore the rare but long trajectories that control the behavior of $M^{(2)}$ in optically thin slabs. In practice the code is run on a supercomputer, which allows to run 30 simulations in parallel, each using 128×10^8 photons (10^9 for directional observations). This amount of photons is needed to capture the divergence of the normalized moments caused by very rare events.

In Figs. 2 and 3, the shaded vertical bars show the histograms of the total paths traveled by photons in the Monte Carlo simulations. This validates the analytical formulas (Eqs. (8), (9), (12), (13)) obtained for collimated and diffuse illumination. Monte Carlo simulations are also used to obtain the pdfs for directional observations (Fig. 4), which again supports the theoretical derivations for sufficiently long paths (Eqs. (32) and (36)).

The ray tracing code is further used to investigate the behavior of the moments at low optical thickness. To this end, the moments are computed for 30 distinct values of τ, ranging from 10^{-6} to 1. These simulations are first used to validate the estimations of the moments derived in Section 2. Figures 5 and 6 show the second and third moments obtained for a slab with $H = 1$ m, for collimated and diffuse illumination. These simulations confirm the formulas derived analytically, in particular Eqs. (39), (40), (42), (45), (46). The same slab is used to simulate directional observations. Figure 7 shows the results for reflectance observations but the results for transmittance observations are not shown since they are redundant with those for reflectance. Again, these simulations confirm the analytical computations for singly and twice-scattered photons, namely Eqs. (50), (54), (55), (57), (58). For angularly integrated reflectance and transmittance observations, the simulations were used to confirm the assumption that singly-scattered photons dominate the 0^{th} moment of $p(l)$, which validates the expressions of the moments derived for these configurations.

Because our analytical derivations do not extend beyond singly or twice-scattered photons, the ray tracing code is used to further explore the τ dependencies for higher orders of scattering. Simulations are also performed for anisotropic scattering, i.e., $g \neq 0$ in the Henyey–Greenstein phase function. These complementary simulations are further discussed in Section 4.

Optics EXPRESS

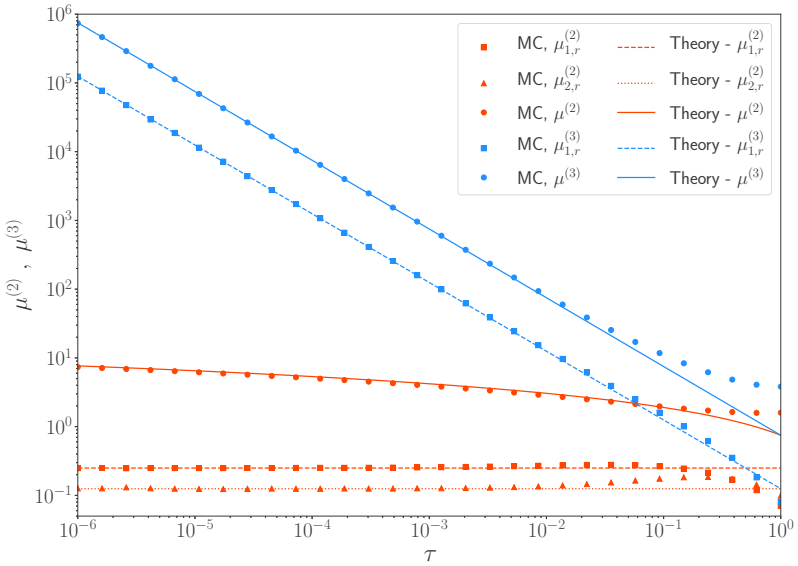

Fig. 6. Same as Fig. 5, but for diffuse illumination ($\mu^{(2)} = M^{(2)}/4H^2$ and $\mu^{(3)} = M^{(3)}/8H^3$). Note that the third moment for twice-scattered photons is not shown because it would superimpose with that of singly-scattered photons.

5. Applications and extensions

5.1. Applications to optical medium measurements

The pdfs derived for singly- and twice-scattered photons (reflected and transmitted) suggest that such measurements (which imply time-resolved measurements) could be used to estimate l_e for optically thin slabs, when low orders of scattering prevail. For instance, Eq. (13) does not depend on H, hence $p_{1,r}(0)$ directly gives access to l_e, meaning that time resolved reflectance measurements could directly provide l_e. In combination with an estimation of H (for instance estimated from the discontinuity of the derivative of $p_{1,r}(l)$ at $l = H(1 + s_0)$, or from the shape of the pdf beyond $H(1 + s_0)$) this could allow to estimate the optical thickness of the slab from a single reflectance measurement. Equivalently, transmittance measurements could be used. In the case the full pdf is not measured, but its second moment is accessible (as in e.g. [10]), the obtained dependence on τ suggests that this fundamental quantity can be estimated even at very low optical thickness. More interestingly, the lower the optical thickness, the larger the variance of the photon path length distribution, suggesting an increased sensitivity to the thinnest media, contrary to what is usually experienced in remote sensing. Although the present study is mostly theoretical, it provides leads for innovative remote sensing studies of optically thin media.

5.2. Higher orders of scattering

For non directional simulations, our analytical calculations did not extend to double scattering. When accounting for double-scattering without under collimated illumination it was shown [23] that at low optical thickness $M^{(2)}_{2,t} \sim H^2/4$ (their Fig. 3), which matched very well their Monte Carlo simulations. Assuming that the pdfs of reflected and transmitted photons have similar tails for a given order of scattering, and assuming that higher-than-two orders of scattering are not significant, this suggests that for collimated illumination:

$$\frac{\mu_0^2 M^{(2)}}{H^2} \sim 1 + \mu_0. \tag{63}$$

Optics EXPRESS

It means that the contributions to the second moment are equally split between single and double-scattering, and between reflected and transmitted scattered paths. Figure 5 shows that this equation perfectly matches the second moments simulated with the ray tracing code. Again following [23] we hypothesize that the contribution of the twice-scattered photons to higher moments is such that:

$$\frac{\mu_0^n M_{2,t}^{(n)}}{H^n} \sim \frac{\mu_0^n M_{2,r}^{(n)}}{H^n} \sim \frac{\mu_0^{n-1}}{4}\tau^{2-n}\Gamma(n), \tag{64}$$

which Fig. 5 also confirms. This overall suggests that:

$$\frac{\mu_0^n M^{(n)}}{H^n} \sim 1 + \frac{\mu_0^{n-1}}{2}\tau^{2-n}\left(\Gamma(n-1) + \Gamma(n)\right). \tag{65}$$

This equation assumes that higher-than-two orders of scattering do not contribute to the asymptotic behavior of the moments, which is again confirmed by Fig. 5 for the third moment.

The same strategy is adopted for diffuse illumination. Contrary to collimated illumination, Monte Carlo simulations suggest that the contribution of twice-scattered photons to the second moment is half that of singly-scattered photons (i.e., $M_{1,r}^{(2)} = 2M_{2,r}^{(2)}$). A possible explanation is that singly-scattered photons with long trajectories include those entering the slab at grazing angles (which can then be scattered in any direction) and those being scattered into the plane. For twice-scattered photons, grazing incident angles do not contribute because the probability to remain within the slab after scattering is very low. On the contrary, for photons already scattered into the plane, the probability to be scattered again before escaping is significant, without changing the overall distance. As already pointed out it seems that both contributions (grazing incident angles and scattering into the plane) are as likely, explaining the factor $1/2$ for twice-scattered photons. As for collimated illumination we can hypothesize that:

$$\frac{M_{2,t}^{(n)}}{2^n H^n} \sim \frac{M_{2,r}^{(n)}}{2^n H^n} \sim \frac{1}{2^{n+1}}\tau^{2-n}\Gamma(n). \tag{66}$$

It implies that the divergence of the second normalized moment in the case of diffuse illumination is only due to directly transmitted photons, while for higher moments directly transmitted, singly-scattered and twice-scattered contribute the same order of magnitude τ^{2-n}, with supposed contributions $\Gamma(n-2)/2^{n-1}$, $\Gamma(n-1)/2^{n-1}$, and $H^n\Gamma(n)/2^n$, respectively. As for collimated illumination, higher orders of scattering are assumed not to dominate the asymptotic behavior. All these expressions and conclusions are supported by the ray tracing simulations, as can be seen in Fig. 6.

For directional observations, the calculations already encompass double scattering. Here we argue that higher orders of scattering are too rare to dominate the asymptotic behavior. Given that singly-scattered photons necessary correspond to short trajectories, it suggests that the overall behavior of the moments is driven by twice-scattered photons. This hypothesis is fully supported by the simulation results shown in Fig. 7.

5.3. Anisotropic scattering

So far, all the calculations presented in this study assumed isotropic scattering. This is an ideal case, poorly representative of actual scattering media. Monte Carlo simulations using an Henyey–Greenstein phase function with $g \neq 0$ suggest that the asymptotic behavior of the moments is unchanged for collimated illumination, except for an offset corresponding to a scaling of the τ dependency. Figure 8 shows the moments computed from the simulations for $g = 0$, $g = 0.5$ and $g = 0.8$ (for collimated illumination with $\mu_0 = 0.8$). In practice, this scaling corresponds to the probability to be scattered into the horizontal plane when coming from the direction θ_0, namely $P(\theta_0, \pi/2)$. For diffuse illumination, the ray tracing simulations

Optics EXPRESS

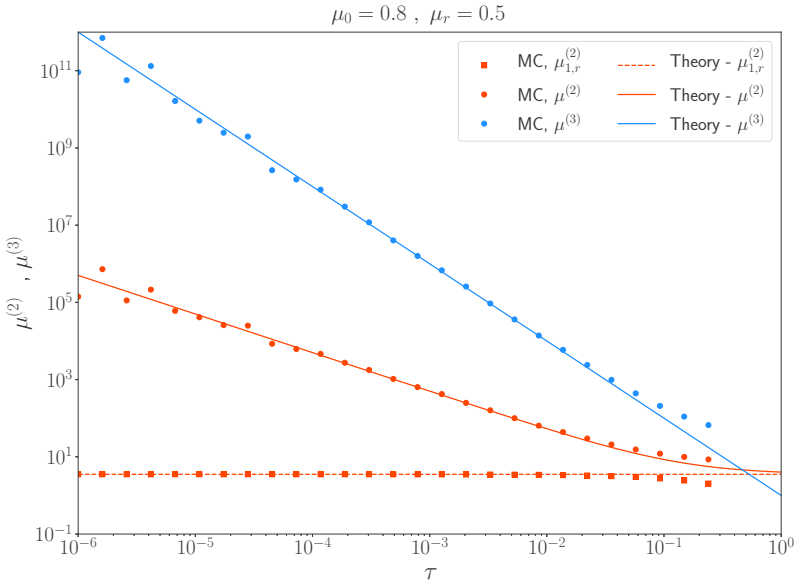

Fig. 7. Same as Fig. 5, but for directional reflectance observations ($\mu_r = 0.5$) under collimated illumination ($\mu_0 = 0.8$). Here $\mu^{(2)} = M^{(2)}/H^2$ and $\mu^{(3)} = M^{(3)}/H^3$.

with anisotropic scattering show that the asymptotic behavior of the moments is exactly the same as for isotropic scattering. In particular the phase function has no impact on $M^{(2)}$ at low optical thickness, because the asymptotic behavior is driven by directly transmitted photons. It

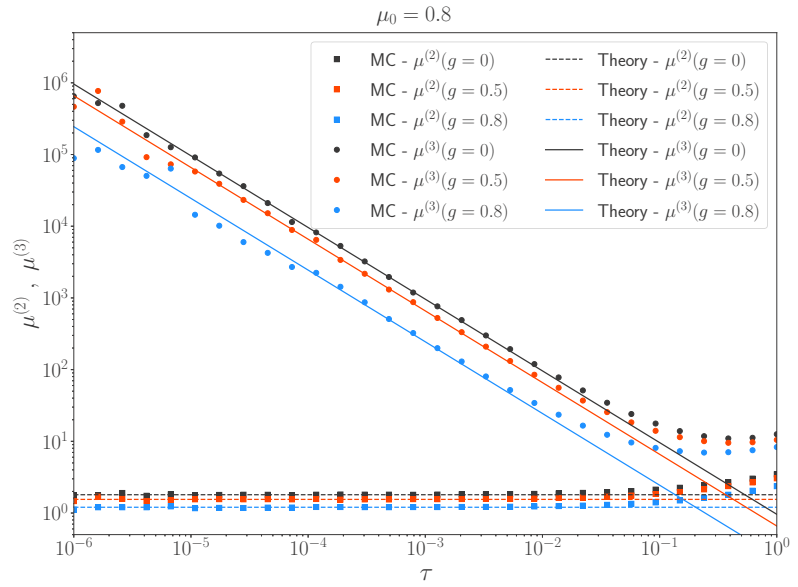

Fig. 8. Same as Fig. 5, but for $\mu_0 = 0.8$ and for 3 different Henyey–Greenstein phase functions ($g = 0$, $g = 0.5$, $g = 0.8$). The lines correspond to a scaling of the paths by $P(\mu_0, \pi/2)$, where this quantity for Henyey–Greenstein phase function is computed after Eq. (76).

Optics EXPRESS

implies that measurements performed in these conditions would directly provide information on the optical thickness, without knowing the phase function, which is an important invariance result. In Appendix B, detailed calculations are performed to support these computational results. When considering directional reflectance or transmittance observations, the scaling includes the contribution of single scattering ($P(\theta_0, \theta_r)$), which determines the 0^{th} moment. The angularly integrated reflectance and transmittance observations are also altered by the impact of the phase function on the 0^{th} moment.

6. Conclusions

Based on comprehensive radiative transfer calculations, we have derived the path length probability distribution functions of singly- and twice-scattered photons, reflected by or transmitted through a homogeneous, non-absorbing, isotropically scattering slab. Various illumination and viewing conditions were investigated, including collimated and diffuse illuminations, and directional reflectance and transmittance configurations. The main focus was on the asymptotic behavior of the distributions and their corresponding moments for optically thin slabs, which have been far less studied than optically thick media.

Under collimated illumination, the second moment of the photon path distribution exceeds the ballistic limit H^2, and the higher order normalized moments diverge as τ^{2-n}. For diffuse illumination, ballistic photons are responsible for the divergence of the second normalized moment as $\ln \tau$, which provides a means to estimate τ from the variance of the distribution. Higher order normalized moments diverge as τ^{2-n}. When only reflected or transmitted photons are considered (under directional or angularly-integrated viewing), the normalized moments diverge as τ^{1-n}, implying that the second normalized moment diverges as τ^{-1}.

Although the detailed calculations are only performed for isotropic scattering, Monte Carlo ray-tracing simulations show that the τ dependency is unchanged for anisotropic scattering, except for a scaling (related to the probability to be scattered parallel to the slab) in the case of collimated illumination. Most interestingly, under diffuse illumination the asymptotic behavior of the moments is insensitive to the phase function. Monte Carlo simulations were also used to explore the impact of higher orders of scattering, confirming that the asymptotic behavior of the moments is dominated by photons scattered once or twice, with contributions of the same order.

In summary, this mostly theoretical work sheds light on a poorly-investigated research topic. As an important application, it provides physical insight to advance the remote sensing of optically thin media. In particular, our results for collimated (and pulsed) sources associated with directional sensors could be applied to (ranged-gated) bistatic lidar systems deployed either on ground (e.g., [27,28]) or in space (e.g., [29]). By contrast, our results for diffuse illumination and angularly-integrated sensing are better suited for the analysis of laboratory measurements.

Appendix A. Detailed calculations of the pdfs for diffuse illumination

A.1 Singly scattered transmitted photons

The integrals over z_0 in Eq. (18) were computed in Section 2.1.1. The first term of the full integral of Eq. (18) is evaluated first:

$$\begin{aligned} I_1 &= \int_{H/l}^{1} \mu_0^2 \left(-\ln\left(1 - \frac{H}{\mu_0 l}\right) - \frac{H}{\mu_0 l} \right) \mathrm{d}\mu_0, \\ &= \frac{1}{l^3} \left(-\frac{1}{3} \left[H^3 \ln\left(\frac{H}{l-H}\right) + \frac{1}{2} H^3 - H^2 l - \frac{1}{2} H l^2 + l^3 \ln\left(\frac{l-H}{l}\right) \right] - \frac{H}{2}(l^2 - H^2) \right). \end{aligned} \tag{67}$$

Optics EXPRESS

The second term reads:

$$\begin{aligned} I_2 &= \int_0^{H/l} \mu_0^2 \left(-\ln\left(\frac{H-\mu_0 l}{l-\mu_0 l}\right) + \frac{l-H}{\mu_0 l}\right) \mathrm{d}\mu_0, \\ &= \frac{1}{l^3}\left(-\frac{1}{3}\left[H^3 \ln\left(\frac{H}{l-H}\right) - \frac{3}{2}H^3 + \frac{1}{2}H^2 l + Hl^2 + l^3 \ln\left(\frac{l-H}{l}\right) - H^4 \ln\left(\frac{l}{H}-1\right)\right] + \frac{l-H}{2}H^2\right). \end{aligned} \tag{68}$$

Equation (19) is obtained by summing both contributions.

A.2 Singly scattered reflected photons

The integrals over z_0 in Eq. (22) were computed in Section 2.1.2. We now compute the integrals over μ_0 for $l \geq 2H$:

$$\begin{aligned} I_1 &= \int_{H/(l-H)}^1 \mu_0^2 \left(\ln\left(1-\frac{H}{\mu_0 l}\right) + \frac{H}{\mu_0 l - H}\right) \mathrm{d}\mu_0, \\ &= \frac{1}{3l^3}\left(l^3 \ln\left(1-\frac{H}{l}\right) - \left(\frac{lH}{l-H}\right)^3 \ln\left(\frac{H}{l}\right)\right. \\ &\left. +2H\left[\frac{1}{2}\left((l-H)^2 - \left(\frac{H^2}{l-H}\right)^2\right) + 2H\left(l - \frac{lH}{l-H}\right) + 2H^2 \ln\left(\frac{l}{H}-1\right)\right]\right). \end{aligned} \tag{69}$$

Likewise,

$$\begin{aligned} I_2 &= \int_0^{H/(l-H)} \mu_0^2 \left(\ln\left(\frac{\mu_0}{1+\mu_0}\right) + \frac{1}{\mu_0}\right) \mathrm{d}\mu_0, \\ &= \frac{1}{3}\left(\left(\frac{H}{l-H}\right)^3 \ln\left(\frac{H}{l}\right) - \frac{1}{2}\left(\left(\frac{l}{l-H}\right)^2 - 1\right) + 2\frac{H}{l-H} - \ln\left(\frac{l}{l-H}\right) + \frac{3}{2}\left(\frac{H}{l-H}\right)^2\right). \end{aligned} \tag{70}$$

Equation (23) is obtained by summing both contributions.

Appendix B. Calculations for anisotropic scattering

Here we demonstrate why anisotropic scattering simply translates into a scaling (with respect to anisotropic scattering) of the moments at low optical thickness for collimated illumination, while it does not alter the moments for diffuse illumination. We expand Eq. (5) in the general case:

$$p(l|z_0)\mathrm{d}l = \frac{H-z_0}{(l-z_0 s_0)^2}\frac{P(\theta_0,\theta_t)}{\sin\theta_t}\mathrm{d}l e^{-\frac{l-l_0}{l_e}}. \tag{71}$$

If we know focus on the long trajectories, since they correspond to scattering in the plane ($\theta_t = \pi/2$) we obtain:

$$\begin{aligned} p_{1,t}(l) &\sim e^{-\frac{l}{l_e}}\frac{s_0}{l_e}\int_0^H \frac{H-z_0}{l^2} P(\theta_0,\pi/2)\mathrm{d}z_0, \\ &\sim \frac{s_0}{2l_e}P(\theta_0,\pi/2)e^{-\frac{l}{l_e}}\left(\frac{H}{l}\right)^2. \end{aligned} \tag{72}$$

Based on this, $M_{1,t}^{(2)} \sim \frac{H^2}{2\mu_0}P(\theta_0,\pi/2)$. Likewise it can be shown that $M_{1,r}^{(2)} \sim \frac{H^2}{2\mu_0}P(\theta_0,\pi/2)$. The validity of this approximation is tested in the case of the Henyey-Greenstein phase function P_{HG}. $P_{\mathrm{HG}}(\theta_0,\phi_0;\theta,\phi)$ corresponds to the probability that light be scattered in direction (θ,ϕ)

Optics EXPRESS

when coming from the direction (θ_0, ϕ_0). This probability only depends on the deviation angle Θ between the incident and scattered directions, and is such that:

$$P_{\mathrm{HG}}(\theta_0, \phi_0; \theta, \phi) = P_{\mathrm{HG}}(\Theta) = \frac{1}{4\pi} \frac{1 - g^2}{\left(1 + g^2 - 2g\cos\Theta\right)^{\frac{3}{2}}}, \tag{73}$$

where g is the asymmetry parameter, defined as:

$$g = \frac{1}{2} \int_0^{\pi} \cos\Theta P_{\mathrm{HG}}(\Theta) \sin\Theta \mathrm{d}\Theta. \tag{74}$$

As for the isotropic case, we define:

$$P_{\mathrm{HG}}(\theta_0, \theta) = \int_0^{2\pi} P_{\mathrm{HG}}(\theta_0, \phi_0; \theta, \phi) \sin\theta \mathrm{d}\phi = \sum_0^{\infty} a_k P_k(\cos\theta_0) P_k(\cos\theta) \sin\theta, \tag{75}$$

where P_k is the k^{th} Legendre polynomial and $a_k = \frac{2k+1}{2} g^k$ [30]. Finally, we have

$$P_{\mathrm{HG}}(\theta_0, \pi/2) = \sum_0^{\infty} \frac{2k+1}{2} g^k P_k(\cos\theta_0) P_k(0), \tag{76}$$

which is the scaling used in Fig. 8 for the theoretical lines.

For diffuse illumination, long trajectories consist of photons scattered in the plane (for any incident angle), and photons which entered the slab at a grazing angle, whatever their direction after scattering. This can be seen as the two terms of Eq. (18). For the first contribution (photons scattered in the plane), we duplicate the computations performed for collimated illumination and integrate over all incident directions, to get (for sufficiently large l values):

$$p_{1,t}(l) \sim \frac{1}{l_e} e^{-\frac{l}{l_e}} \left(\frac{H}{l}\right)^2 \int_0^{\pi/2} P(\theta_0, \pi/2) \sin\theta_0 \mathrm{d}\theta_0. \tag{77}$$

Using the expansion of $P(\theta_0, \pi/2)$ in Legendre polynomials, and the fact that $P_k(0) = 0$ for odd k, and that for even k>0, P_k is symmetric and averages to 0, we obtain:

$$\int_0^{\pi/2} P(\theta_0, \pi/2) \sin\theta_0 \mathrm{d}\theta_0 = \int_0^1 \sum_{k=0}^{\infty} a_k P_k(\mu_0) P_k(0) \mathrm{d}\mu_0 = a_0. \tag{78}$$

For grazing angles ($\theta_0 \sim \frac{\pi}{2}$), we first note that $\sin\theta_t \mathrm{d}\theta_t = \mathrm{d}z_0 \frac{Hs_0 - l}{(l - z_0 s_0)^2} \sim \mathrm{d}z_0 s_0 \frac{H - z_0}{(l - z_0 s_0)^2}$, where we have used the fact that $l \sim l_0$. Hence we can use the variable θ_t for the integration instead of z_0 as follows:

$$\int_0^{H/l} \int_0^{(l-H)/(s_0-1)} \frac{H - z_0}{(l - z_0 s_0)^2} \frac{p(\pi/2, \theta_t)}{\sin\theta_t} \mathrm{d}z_0 \mathrm{d}\mu_0 \sim \int_0^{H/l} \int_0^1 2\mu_0 P(\pi/2, \theta_t) \mathrm{d}\theta_t \mathrm{d}\mu_0 \sim a_0 \frac{H^2}{l^2}, \tag{79}$$

where we've again used the properties of the Legendre polynomials to get $\int_0^1 P(\pi/2, \theta_t) \mathrm{d}\theta_t = a_0$. It suggests that the contribution of grazing photons is similar to that of photons scattered in the plane. This is consistent with the fact that $I_1 \sim I_2$ (Eqs. (67) and (68)) for isotropic scattering and the physical explanation presented in the main text to explain the different contributions of single and twice-scattered photons. Overall, for diffuse illumination, the scaling equals $2a_0 = 1$ whatever the phase function, because $a_0 = \frac{1}{2}$ corresponds to the normalization of the phase function. This highlights the total insensitivity of the asymptotic behavior of the moments to the details of the phase function, and in particular to g. Note that the same conclusions could be obtained for reflected paths.

Optics EXPRESS

Funding. Institut national des sciences de l'Univers (LEFE CASPER); NASA Science Mission Directorate (105357, EPIC CLOUD ALGORITHMS).

Acknowledgments. This work was supported by the French national programme LEFE/INSU through the CASPER project. This work was partially carried out at the Jet Propulsion Laboratory, California Institute of Technology, under a contract with the National Aeronautics and Space Administration (80NM0018D0004). AD is supported by NASA's SMD/ESD DSCOVR mission (EPIC CLOUD ALGORITHMS, Project: 105357, Task: 239702.04.32.01.13, HQs PM Richard S. Eckman). QL thanks Ghislain Picard and Nicolas Ferlay for rich discussions on this topic.

Disclosures. The authors declare no conflicts of interest.

Data availability. Data underlying the results presented in this paper are available in Ref. [31].

References

1. W. M. Irvine, "The formation of absorption bands and the distribution of photon optical paths in a scattering atmosphere," Bull. Astronom. Inst. Netherlands **17**, 266 (1963).
2. T. Svensson, E. Alerstam, J. Johansson, and S. Andersson-Engels, "Optical porosimetry and investigations of the porosity experienced by light interacting with porous media," Opt. Lett. **35**(11), 1740–1742 (2010).
3. M. Allgaier, M. G. Cooper, A. E. Carlson, S. W. Cooley, J. C. Ryan, and B. J. Smith, "Direct measurement of optical properties of glacier ice using a photon-counting diffuse lidar," J. Glaciol. pp. 1–11 (2022).
4. Q. Libois, F. Lévesque-Desrosiers, S. Lambert-Girard, S. Thibault, and F. Domine, "Optical porosimetry of weakly absorbing porous materials," Opt. Express **27**(16), 22983–22993 (2019).
5. J. F. Appleby and W. M. Irvine, "Path-length distributions of photons diffusely reflected from a semi-infinite atmosphere," The Astrophys. J. **183**, 337–346 (1973).
6. R. D. Skocypec and R. O. Buckius, "Photon path length distributions for an isotropically scattering planar medium," J. Quant. Spectrosc. Radiat. Transf. **28**(5), 425–439 (1982).
7. T. Scholl, K. Pfeilsticker, A. B. Davis, H. Klein Baltink, S. Crewell, U. Löhnert, C. Simmer, J. Meywerk, and M. Quante, "Path length distributions for solar photons under cloudy skies: Comparison of measured first and second moments with predictions from classical and anomalous diffusion theories," J. Geophys. Res. **111**(D12), D12211 (2006).
8. H. C. Van de Hulst, Multiple Light Scattering (Academic, 1980).
9. C. Zeller and R. Cordery, "Light scattering as a Poisson process and first-passage probability," J. Stat. Mech. **2020**(6), 063404 (2020).
10. L. Harrison and Q. Min, "Photon pathlength distributions from O_2 A-band absorption," in *Proceedings of the International Radiation Symposium*, August, (1996), pp. 19–24.
11. M. S. Patterson, B. Chance, and B. C. Wilson, "Time resolved reflectance and transmittance for the noninvasive measurement of tissue optical properties," Appl. Opt. **28**(12), 2331–2336 (1989).
12. A. B. Davis, N. Ferlay, Q. Libois, A. Marshak, Y. Yang, and Q. Min, "Cloud information content in EPIC/DSCOVR's oxygen A-and B-band channels: A physics-based approach," J. Quant. Spectrosc. Radiat. Transf. **220**, 84–96 (2018).
13. Q. Min and L. Harrison, "Joint statistics of photon pathlength and cloud optical depth," Geophys. Res. Lett. **26**(10), 1425–1428 (1999).
14. L. Mei, G. Somesfalean, and S. Svanberg, "Light propagation in porous ceramics: Porosity and optical property studies using tunable diode laser spectroscopy," Appl. Phys. A **114**(2), 393–400 (2014).
15. S. Blanco and R. Fournier, "An invariance property of diffusive random walks," Europhys. Lett. **61**(2), 168–173 (2003).
16. R. Savo, R. Pierrat, U. Najar, R. Carminati, S. Rotter, and S. Gigan, "Observation of mean path length invariance in light-scattering media," Science **358**(6364), 765–768 (2017).
17. S. Blanco and R. Fournier, "Short-path statistics and the diffusion approximation," Phys. Rev. Lett. **97**(23), 230604 (2006).
18. A. B. Davis, R. F. Cahalan, D. Spinehirne, M. J. McGill, and S. P. Love, "Off-beam lidar: An emerging technique in cloud remote sensing based on radiative Green-function theory in the diffusion domain," Phys. Chem. Earth, Part B: Hydrol. Ocean. Atmosphere **24**(3), 177–185 (1999).
19. A. B. Davis and A. Marshak, "Space-time characteristics of light transmitted through dense clouds: A Green's function analysis," J. Atmos. Sci. **59**(18), 2713–2727 (2002).
20. L. Pattelli, G. Mazzamuto, D. S. Wiersma, and C. Toninelli, "Diffusive light transport in semitransparent media," Phys. Rev. A **94**(4), 043846 (2016).
21. C. R. Doering, T. S. Ray, and M. L. Glasser, "Long transmission times for transport through a weakly scattering slab," Phys. Rev. A **45**(2), 825–828 (1992).
22. M. Boguná, J. M. Porra, and J. Masoliver, "Persistent random walk model for transport through thin slabs," Phys. Rev. E **59**(6), 6517–6526 (1999).
23. T. S. Ray, M. L. Glasser, and C. R. Doering, "Anomalous transmission-time moments in the ballistic limit of isotropic scattering," Phys. Rev. A **45**(12), 8573–8579 (1992).
24. Q.-L. Min, L. C. Harrison, P. Kiedron, J. Berndt, and E. Joseph, "A high-resolution oxygen A-band and water vapor band spectrometer," J. Geophys. Res. **109**(D2), D02202 (2004).

Optics EXPRESS

25. L. Wang, S. L. Jacques, and L. Zheng, "MCML—Monte Carlo modeling of light transport in multi-layered tissues," Comput. Methods Programs Biomed. **47**(2), 131–146 (1995).
26. L. G. Henyey and J. L. Greenstein, "Diffuse radiation in the galaxy," The Astrophy. J. **93**, 70–83 (1941).
27. J. A. Reagan, D. M. Byrne, and B. M. Herman, "Bistatic lidar: A tool for characterizing atmospheric particulates: Part i—the remote sensing problem," IEEE Trans. Geosci. Remote Sensing **GE-20**(3), 229–235 (1982).
28. J. E. Barnes, N. P. Sharma, and T. B. Kaplan, "Atmospheric aerosol profiling with a bistatic imaging lidar system," Appl. Opt. **46**(15), 2922–2929 (2007).
29. M. D. Alexandrov and M. I. Mishchenko, "Information content of bistatic lidar observations of aerosols from space," Opt. Express **25**(4), A134–A150 (2017).
30. J. I. Jiménez-Aquino and J. R. Varela, "Two stream approximation to radiative transfer equation: An alternative method of solution," Rev. Mex. Fis. **51**, 82–86 (2005).
31. Q. Libois, "Monte Carlo ray tracing code and simulations for photons scattered by an optically thin slab," Zenodo(2022), https://zenodo.org/record/6744097